PAPER

Voyager Radio Science: Observations and Analysis of Neptune's Atmosphere

Ei-ichi MIZUNO†*, *Member*, **Nobuki KAWASHIMA**††, *Nonmember*, **Tadashi TAKANO**††, *Member and* **Paul A. ROSEN**†, *Nonmember*

SUMMARY Voyager Neptune radio science data were collected using three antennas on Earth on August 25, 1989. A parabolic antenna at Canberra, Australia, of 70 meter diameter received 2.3 GHz and 8.4 GHz carriers. The 64 meter parabolic antennas at Parkes. Australia and Usuda, Japan, received only the 8.4 GHz and only the 2.3 GHz carriers, respectively. It is necessary to reduce the frequency variation in the received signal carrier to extract accurate information on physically interesting objects such as Neptune's atmosphere, ionosphere, or the rings. After the frequency stabilization process, the frequency drift was reduced from $\sim$ 180 Hz down to a maximum of $\sim$ 5 Hz, making it possible to reduce the data bandwidth and, consequently, the data volume, by a factor of 30. The uncertainty of the signal frequency estimates were also reduced from $\sim$5 down to 5×10^{-3} Hz/sec above the atmosphere, from $\sim$5 down to 0.5 Hz/sec in the atmosphere, and from $\sim$50 down to $\sim$3 Hz/sec at the beginning and the end of the atmospheric occultation. Much of the remaining uncertainty is due to scintillations in Neptune's atmosphere and cannot be reduced further. The estimates are thus meaningfully accurate and suitable for scientific analysis and coherent arraying of data from different antennas. Two results based on these estimates are shown: a preliminary temperature-pressure ($T-p$) profile of Neptune's atmosphere down to a pressure level of $\sim$2 bar computed using the Usuda 2.3 GHz data, and a multipath phenomenon in the atmosphere seen in Canberra 8.4 GHz data. Our $T-p$ profile shows good agreement with the results presented by Lindal et al.[1] within 1 K below 100 mbar pressure level, even though our result is based on an independent data set and processing. A comparison of the multipath phenomena at Neptune with that at Uranus[2] implies that it was created by a cloud layer with a smaller scale height than the atmosphere above and below it. The processing methods described were developed in part with the interest to coherently array Canberra, Parkes and Usuda data[3]. In this sense, while this paper does not extend any science results, the observations and results are derived independently from other published results, and in the case of Usuda, are completely new.

key words: *voyager neptune encounter, atmospheric multipath, radio occultation, temperature-pressure profile*

1. Introduction

Radio science observations of Neptune were performed during the period of Voyager 2's occultation by the Neptunian system on August 25, 1989. For these observations, unmodulated carriers of 2.3 and 8.4 GHz, excited by a highly phase-stable oscillator on Voyager*, were transmitted from the spacecraft toward the earth. Three independent parabolic antennas located on Earth (Table 1) were used to receive these signals.

Radio science observations are in essence the frequency (or phase) and the amplitude modulations in the received carrier induced when the transmitted unmodulated carrier propagates through a medium of interest such as the atmosphere, ionosphere or rings of a planet. Table 2 presents the desired radio science analysis goals and the required observables. The radio science technique has been used to derive for example, temperature and pressure of the atmosphere, electron density of the ionosphere, or the structure of the ring system at many planets in our solar system[4]-[7].

This paper describes our method of extracting the signal frequency and amplitude from the Voyager

Table 1 Receiving stations for Voyager Neptune radio science observations.

Location	Diameter	Receiving frequency
Canberra (Australia)	70 m	2.3 and 8.4 GHz
Parkes (Australia)	64 m	8.4 GHz
Usuda (Japan)	64 m	2.3 GHz

Table 2 Radio science data analysis and the observables needed.

Analysis	Used Observables
Electron density profile of ionosphere	Phase
Temperature-pressure profile of atmosphere	Frequency
Absorption in the atmosphere	Frequency and amplitude
Multipath phenomena by a cloud layer	Power spectrum
Ring structure	Phase and Amplitude
Particle size distribution of the rings	Power spectrum
Small scale structure in the atmosphere	Amplitude

Manuscript received January 7, 1990.
Manuscript revised September 23, 1991.

† The authors are with the Faculty of Engineering, Kanazawa University, Kanazawa-shi, 920 Japan.
†† The authors are with Institute of Space and Astronautical Science, Sagamihara-shi, 229 Japan.
* Presently, with Institute of Space and Astronautical Science.

* This crystal oscillator is called an Ultra Stable Oscillator (USO).

Neptune radio science data, presents the magnitude of all the possible errors affecting the frequency estimates, and gives some examples of the data and derived physical quantities. A detailed description of the receiver and recorder systems can be found in Ref. (8). Here we stress the methods employed to convert the received raw data into a basic data set useful for scientific analysis. The techniques are based largely on those developed for previous studies[4],[9],[10]. However, this work includes certain extensions and new aspects for this experiment, being the first trial in Japan.

In Sec. 2, we briefly summarize how the data were recorded, focussing on the signal frequency conversion process and the possible error sources which affect the frequency estimates. In Sec. 3, we discuss how to extract the frequency and amplitude of the signal from the received data. In Sec. 4, we use these estimates to show two preliminary results, the temperature-pressure ($T-p$) profile of Neptune's atmosphere and a multipath phenomenon found in the atmosphere. In Sec. 5, we discuss the results presented in this paper, and introduce our next target using these data.

2. Experiment System and Data Characteristics

2. 1 Data Generation Method

At the three antennas, received data were digitally recorded in real time with 8 bit quantization and sampling rates of 50 kHz for Canberra 2.3 and 8.4 GHz signals, and 80 kHz for Parkes 8.4 GHz and Usuda 2.3 GHz signals†. Open-loop receivers convert the signal frequencies at the antennas (antenna frequencies) down to these digital recording frequency bands, so as not to disturb the frequency (or phase) and amplitude information of the signal. In a closed-loop system such as a phase locked loop receiver, the received frequency is adjusted automatically to maintain it in the recording passband. In this process the true frequency, including modulations due to the media under study, is lost. In contrast, the tuning history of the Voyager-Neptune open-loop receivers was preserved so that no frequency information was lost[8]. Because accurate estimation of the signal frequency is so critical to radio science objectives, it is important to clarify the components that comprise the recorded frequency, and the procedures by which the frequency components are estimated to extract physical properties of interest.

2. 2 Frequency Considerations

The antenna frequency can be written as

$$f_{\mathrm{ant}}(t)=f_{\mathrm{pred}}(t)+f_{\mathrm{unmodelled}}(t) \qquad (1)$$

where f_{pred} is the predicted and $f_{\mathrm{unmodelled}}$ is the unknown part. The frequency f_{pred} can be written as

$$f_{\mathrm{pred}}(t)=f_{\mathrm{USO}}+f_{\mathrm{dopp}}(t)+f_{\mathrm{atm}}(t) \qquad (2)$$

where f_{USO} is the transmitted signal frequency at the spacecraft, f_{dopp} is a prediction of the doppler frequency due to relative motion and relativistic effects, and f_{atm} a prediction of the doppler perturbation due to refraction by the atmosphere of Neptune. The frequency f_{dopp} is computed from the best estimates of the positions and velocities of the spacecraft and the receiving station, and the masses of the bodies involved. The frequency f_{atm} is computed from a model atmosphere.

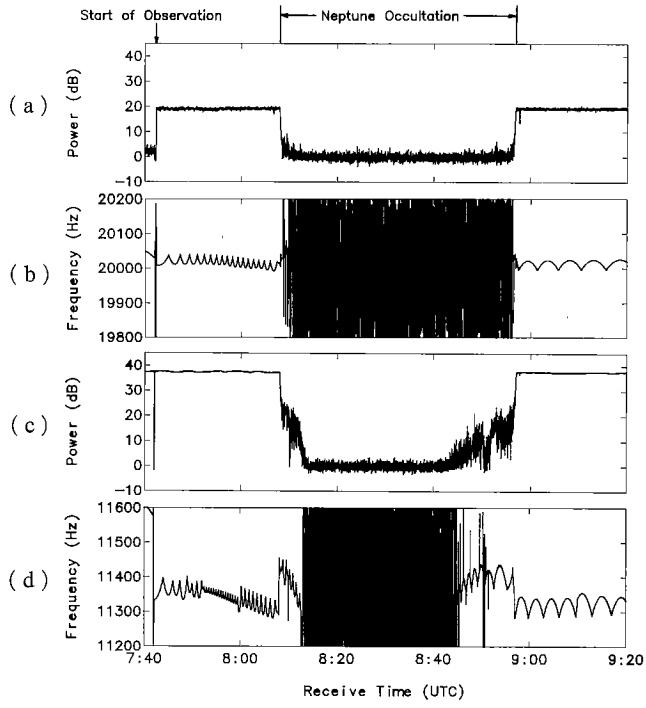

Fig. 1 Received relative signal power and frequency profiles for Usuda 2.3 GHz (a),(b) and Canberra 8.4 GHz (c),(d) signals around Neptune occultation. In (a) and (b), noise levels are adjusted to 0 dB, for convenience. Neptune occultation, from 8 : 08 to 8 : 57, is the time interval from the raypath started penetrating the Neptune's atmosphere. As the raypath goes deeper into the atmosphere, the received signal power (a),(c) becomes lower mainly due to defocussing. Two sharp drops of the signal level at 8 : 10 and 8 : 51 are due to the strong defocussing and microwave absorption by a methane cloud layer. Received signal frequency (b),(d) shows a quasi-periodic frequency drift due the receiver. When the signal is below the noise level, the signal frequency has no meaning. These profiles are computed using the method described in Appendix. We note that the frequency accuracy in the Neptune's atmosphere here is ~50 Hz in the worst case (see Sec. 3. 1). Used integration times here are 0.8192 sec for Usuda and 0.65536 sec for Canberra data, respectively.

† Their final filtering bandwidths at −3 dB level were 20 kHz for Canberra and 35 kHz for Parkes and Usuda data.

During the Voyager Neptune observation, f_{ant} changed by about 80 kHz for the 2.3 GHz signal and about 300 kHz for the 8.4 GHz signal, mainly due to changes in $f_{dopp}(t)$ and $f_{atm}(t)$. These frequency changes are larger than the digital recording bandwidths shown above. The information in f_{pred} was used to create a local signal to mix to the received signal at the intermediate frequency stage such that the output signal frequency at the last stage before digitization was around the middle of the passband. The recorded signal frequency is

$$f_{rec}(t) = f_{ant}(t) - f_{tun}(t), \qquad (3)$$

where f_{tun} is a piecewise linear approximation of f_{pred} and represents the total frequency offset in the receiver after all stages of heterodyning.

Figure 1 shows f_{rec} for (b) the Usuda 2.3 GHz and (d) the Canberra 8.4 GHz signal around the period of the occultation by Neptune. The signal frequency is not exactly constant, but stable enough for recording in the passbands for both signals. The quasiperiodic artificial frequency drift is mainly due to the piecewise linear approximation of f_{pred}. Other random variations are the effects of $f_{unmodelled}$.

2. 3 Components of the Recorded Frequency

Table 3 lists the possible causes of the frequency drift in f_{rec} based on the Canberra 8.4 GHz signal. The main effects are the error of the piecewise linear approximation to the predict in the receiver ($f_{pred} - f_{tun}$), of the order of ~50 Hz, the spacecraft and receiving station trajectory errors Δf_{dopp}, of the order of ~2 Hz, and Neptune's model atmosphere error Δf_{atm}, of the order of ~150 Hz. Of the three, ($f_{pred} - f_{tun}$) can be computed directly from the predict f_{pred} and f_{tun}, which is recorded with the data themselves, and so can be removed completely. This procedure will be discussed in Sect. 3. 2. To estimate Δf_{dopp} and Δf_{atm}, we would need to iteratively solve for the trajectory of Voyager 2 and the raypath in Neptune's atmosphere together by ray tracing. It is not impossible to accomplish this rigorously, but a lot of effort is required. We could use the same iterative method to compute Δf_{ei} and Δf_{ea} due to Earth's ionosphere and atmosphere. Of the remaining effects in Table 3, Δf_{im}, Δf_{clock}, and Δf_{USO} are random, and therefore not predictable, but small. The last effect Δf_{apc} is well-modelled for the Canberra antanna, however, no such model is available for the Parkes or Usuda antennas. From these facts, we understand that

Table 3 Various sources of the signal frequency drift which appears in f_{rec} in Sect. 2 are shown. The data is based on Canberra 8.4 GHz data. Of the shown sources, f_{pred} is known and f_{tun} has been recorded on mgnetic tapes with the digitally recorded signals in real time. The error Δf_{dopp} is computed from the uncertainty in the trajectory of Voyager 2 near Neptune, which is $\Delta t \sim 0.009$ seconds in terms of time[11]. We can see the amount of Δf_{atm} from Fig. 3(a). The approximate relation of $f_{apc} \approx -2.0 \cos\theta \cdot \partial\theta/\partial t$ is known, for Canberra antenna, where t is time in seconds and θ is the elevation angle of the antenna in radian[12]. A similar relation for Canberra 2.3 GHz data is known. However, no such relation is available for Parkes or Usuda antenna. There also exist models for the propagation delay due to earth's neutral atmosphere and ionosphere. The estimation of Δf_{ea}, and Δf_{ei} are based on the simple model shown in Ref. (13), both for the elevation angle of ~60°. For Δf_{im}, we simply extrapolated the doppler scintillation data in Ref. (14). Δf_{clock}[15] and Δf_{USO}[16], clock stabilities, are unpredictable. Using this notation, $f_{unmodelled}$ in Sect. 2. 2 becomes $f_{unmodelled} \approx \Delta f_{dopp} + \Delta f_{atm} + \Delta f_{ei} + \Delta f_{ea} + \Delta f_{im} + \Delta f_{clock} + \Delta f_{USO} + \Delta f_{apc}$.

Effects	Notation in this paper	Order (Hz)	Frequency Dependence	Type of variation	Predictable or not
(Real predict)−(Ramp approximation)	$f_{pred} - f_{tun}$	~ 50	$\propto f_{ant}^{0}$	Systematic	Predictable
Spacecraft trajectory error	Δf_{dopp}	~ 2	$\propto f_{ant}$	Systematic	Not
Neptune atmosphere model error	Δf_{atm}	~ 150	$\propto f_{ant}$	Quasi Random	Not
Ray bending due to the earth's ionosphere	Δf_{ei}	$\sim 9 \times 10^{-2}$	$\propto f_{ant}^{-1}$	Quasi Random	Partly Predictable
Ray bending due to the earth's atmosphere	Δf_{ea}	$\sim 2 \times 10^{-3}$	$\propto f_{ant}$	Quasi Random	Partly Predictable
Interplanetary media	Δf_{im}	$\sim 5 \times 10^{-3}$	$\propto f_{ant}^{-1}$	Random	Not
Stability of receiving station clock	Δf_{clock}	$\sim 8 \times 10^{-5}$	$\propto f_{ant}^{0}$	Random	Not
Stability of the spacecraft clock	Δf_{USO}	$\sim 2 \times 10^{-2}$	$\propto f_{ant}$	Random	Not
The motion of antenna phase center	Δf_{apc}	$\sim 6 \times 10^{-5}$	$\propto f_{ant}$	Systematic	Partly Predictable

the only effect that can be removed completely is $(f_{\text{pred}} - f_{\text{tun}})$. Therefore, for simplicity, we treat all the other effects as though they were unseparable and unmodellable effects. In Sect. 3. 3, we try to remove the aggregate using the time series of the drifting signal frequency itself after $(f_{\text{pred}} - f_{\text{tun}})$ is removed.

3. Frequency Determination Procedure

3. 1 Overview of Data Reduction

The received signal is basically a noisy sinusoid with time-varying frequency and amplitude caused by the perturbing medium of interest. The SNR of the Canberra 8.4 GHz signal during this experiment (Fig. 1(c)) was as high as 45 dB·Hz above the atmosphere, and 20 dB·Hz even below the methane cloud layer ($\sim$8 : 10). Under such high SNR conditions, the standard deviation of the estimated signal frequency was $\sigma_f \approx 10^{-2} \sim 10^{-4}$(Hz). On the other hand, the received signal frequency (Fig. 1(d)) drifted with the rate of $\sim$5 Hz/sec both in and above the atmosphere, except for the instants when the occultation by the atmosphere started ($\sim$8 : 08 : 10) and ended ($\sim$8 : 56 : 50), where the remaining sudden frequency drifts became as rapid as $\sim$50 Hz/sec. To estimate the signal frequency, we use a robust technique which essentially computes the discrete Fourier transform (DFT) of data and searches for the frequency with the maximum power in a power spectrum (see Appendix). In a typical required DFT integration time of $T \approx 0.5 \sim 3$ sec, the frequency drifts by $\Delta f_{\text{rate}} \approx 2.5 \sim 15$ Hz, which is much larger than σ_f. The estimated signal power also becomes inaccurate as frequency drift becomes larger for a given integration time. Therefore, stabilization of the signal frequency is necessary so that the estimation be accurate.

Figure 2 is a flow diagram illustrating our method to remove the frequency drift in the received signal. At first ($N=1$), some frequency drift in the original data is removed using the predictable information $(f_{\text{pred}} - f_{\text{tun}})$ (Sect. 3. 2) and then the signal frequency is estimated. The data are bandpass filtered and at the same time decimated according to the maximum frequency variation still remaining. The filtering scheme automatically converts the data to a complex, or "analytic signal", representation in which each datum comprise the amplitude and phase of a sinusoidal signal with noise[3]. The sampling frequency of the complex data is half that of the real data. If the signal frequency is stable enough there, data reduction is complete. Typically it is not stable enough because of the factors affecting frequency discussed in Sect. 2. 3. The stabilization stages for $N>1$ are empirical (Sect. 3. 3), using the signal frequency estimates themselves from the previous stage. The loop is continued until the signal frequency becomes sufficiently stable. Sufficient stability is achieved when the systematic frequency trends are smaller than the frequency noise standard deviation. By "noise", we mean either thermal and oscillator noise, or the scintillation introduced by the atmosphere. We note that the antenna frequency can be reconstructed at any stage because we preserve the history of the frequency variations removed from the data.

3. 2 Predictable Frequency Compensation

The frequency drift $(f_{\text{pred}} - f_{\text{tun}})$ can be removed in the following way. At first, we divide the total time period of the received signal into many small time intervals. In each interval, we approximate $(f_{\text{pred}}(t) - f_{\text{tun}}(t))$ by a third-order polynomial, keeping the frequencies at the two boundaries continuous with the

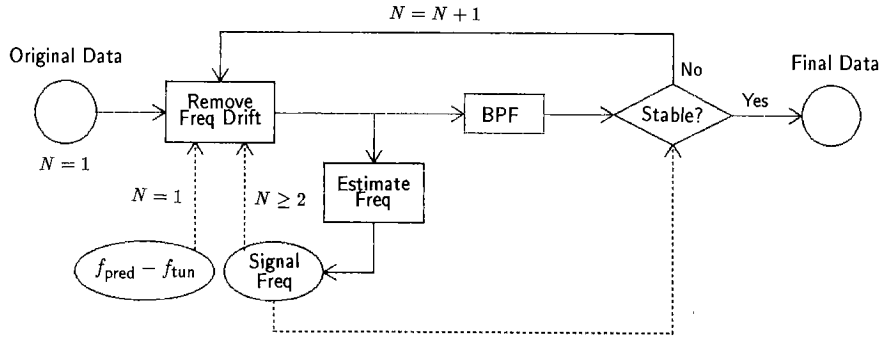

Fig. 2 A flow diagram of the procedure to extract signal frequency information from the received data. Rectangles indicate operations on the occultation data themselves, circles occultation data products, and ovals derived parameters or auxiliary inputs. Solid lines indicate data flow, and dashed lines inputs of auxiliary data. The digital bandpass filter shown here not only filters the data but also reduces the data volume according to the resultant passband. The procedure to estimate the frequency is discussed in Appendix.

adjacent intervals. Let us define this set of polynomials as $f_{\text{steer1}}(t)$. The time intervals need to be small enough so that the error $\Delta f_{\text{steer1}}(t)=|f_{\text{steer1}}(t)-f_{\text{pred}}(t)+f_{\text{tun}}(t)|$ produced by this approximation be smaller than any of the effects in $f_{\text{unmodelled}}$. In our case, the interval is on the order of ~30 seconds. Next, we multiply every complex datum by

$$c_{\text{steer1}}(t)=e^{-2\pi i}\int(f_{\text{steer1}}(t)-f_{\text{center}})\,dt \qquad (4)$$

where f_{center} is half the sampling frequency of the complex data, placing the carrier in the center of the passband. As a result, the signal frequency becomes

$$f_1(t)=f_{\text{center}}+f_{\text{unmodelled}}(t) \qquad (5)$$

where we assume $\Delta f_{\text{steer1}}(t)\approx 0$. Figure 3(a) shows the profile of $f_1(t)$. If the value of $f_{\text{unmodelled}}$ is zero, this value becomes f_{center}, a constant value. However, as is seen in the figure, it varies on the order of 150 Hz, and we can only know it from the data themselves.

3.3 Empirical Compensation of the Signal Frequency

For empirical compensation we compute the polynomials using the data themselves. Because we are using a DFT to compute the signal frequency (see Appendix), when the SNR is low this method sometimes regards noise as signal. In such a case, there can appear a large sudden frequency jump. An example of this in Fig. 1(d) and Fig. 3(a) and (b) around 08: 10: 00 occurs because the signal power abruptly becomes low due to microwave defocussing and/or absorption by the methane layer in Neptune's atmosphere. If we include such a large frequency error in fitting a polynomial, it will cause a large error in the result. Therefore, we used the following method so that we only fit statistically normal points.

After fitting a set of third-order polynomials f_{steer2} to all points in the time series of the signal frequency $f_1(t_k)$, we compute the residual

$$\sigma=\sqrt{\sum_{k=1}^{N}|f_1(t_k)-f_{\text{steer2}}(t_k)|^2/N}. \qquad (6)$$

If there exists any sample time t_n at which the deviation $|f_1(t_n)-f_{\text{steer2}}(t_n)|$ exceeds a constant β times the residual, we exclude the sample and recompute f_{steer2}. When no such points exist, the iterations are complete. We choose the constant β empirically. A value of 2~2.5 gives reasonable results.

We then multiply the data by $c_{\text{steer2}}(t)$, defined analogously to $c_{\text{steer1}}(t)$ of Eq. (4). As a result, the signal frequency $f_2(t)=f_1(t)-f_{\text{steer2}}(t)$ becomes more stable than $f_1(t)$. Using f_2, we compute a newer set of polynomials $f_{\text{steer3}}(t)$ again and remove the frequency drift in the same way. Then the signal frequency becomes $f_3(t)=f_2(t)-f_{\text{steer3}}(t)$. We repeat this procedure to make the resultant signal frequency as stable as possible (see Sect. 3. 1 and Fig. 2). Figure 3(b) shows the final result after 3 iterations of this procedure. The frequency change rate is reduced down to $\Delta f_{\text{rate}}\approx 5\times 10^{-3}$ Hz/sec above the atmosphere, $\Delta f_{\text{rate}}\approx 0.5$ Hz/sec in the atmosphere, and $\Delta f_{\text{rate}}\approx 3$ Hz/sec at the start and the end of the atmosphere occultation.

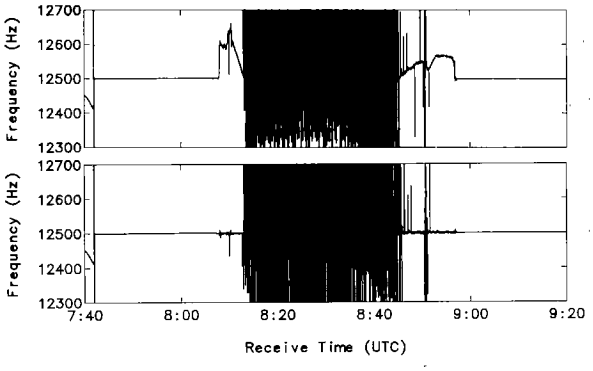

Fig. 3 Signal frequency profile showing the frequency stabilization process. (a) shows the signal frequency after ($f_{\text{pred}}-f_{\text{tun}}$) is subtracted. A frequency drift as large as 150 Hz still remains. (b) shows the signal frequency after the remaining frequency drift is empirically removed.

4. Results of Data Analysis

4.1 Temperature-Pressure Profile of Neptune's Atmosphere

Once we compute the signal frequency and amplitude accurately using the data, we can determine the temperature-pressure ($T-p$) profile of Neptune's neutral atmosphere.

The net frequency perturbation due to ray bending by Neptune's atmosphere is given by $(f_{\text{atm}}+\Delta f_{\text{atm}})$. This information and the trajectory of Voyager 2, Neptune, Sun, and the Earth, are sufficient to compute the ray bending angle α versus ray closest approach distance a[4],[17]. We compute α versus a assuming that the atmosphere of Neptune is spherically symmetric. The refractive index $\mu(r)$, where r is the distance from the center of the planet, derives from Abel's integral inversion of $\alpha(a)$[17]. Next, we can convert the refractive index profile $\mu(r)$ into the molecular number density profile $n(r)$ since the mean molecular number density of a gas is proportional to its average electric dipole polarizability[2],[18]. $\mu(r)$ can be converted into mass density profile $\rho(r)$ if we know the composition of the atmosphere. The pressure profile $p(r)$ of the atmosphere then may be determined using the equation of hydrostatic equilibrium. Finally, we can compute the temperature $T(r)$ of the atmosphere from $n(r)$ and $p(r)$ using the ideal gas law.

As was discussed in Sect. 2. 3, it is difficult to separate Δf_{atm} from other unmodelled effects Δf_{dopp},

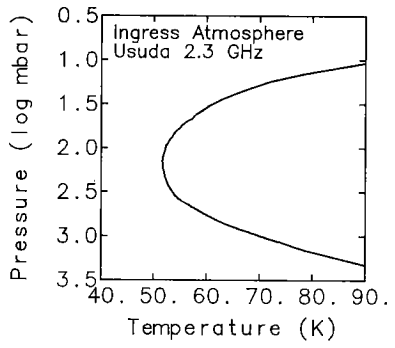

Fig. 4 Temperature-pressure profile of Neptune's atmosphere. This profile was computed using the Usuda 2.3 GHz data for the period of ingress atmosphere occultation assuming a spherically symmetric atmosphere of Neptune (see text).

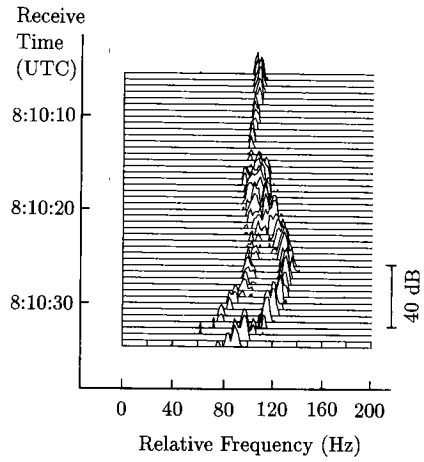

Fig. 5 Power spectra of the signal around the multipath region, computed using the Canberra 8.4 GHz data after removing the effect of $(f_{\text{pred}}-f_{\text{tun}})$ (corresponding to Fig. 3 (a)). The remaining gradual frequency drift, especially after 8 : 10 : 20, is due to $f_{\text{unmodelled}}$.

Δf_{ei}, Δf_{ea}, Δf_{im}, Δf_{clock}, Δf_{USO}, and Δf_{apc}. Therefore, the unseparable effects together with the estimation errors of the estimated signal frequency σ_f and the frequency drift Δf_{rate} are the error sources in analyzing Neptune's atmosphere. Here we note that the error in the estimated frequency propagates to the $\alpha(a)$ profile where it is integrated to compute the refractive index, and then integrated again to compute the pressure or temperature of Neptune, implying that a systematic frequency error can cause a large error in the derived physical properties. Accurate estimate of the signal frequency, therefore, is important.

Figure 4 shows a $T-p$ profile of Neptune's atmosphere computd from Usuda 2.3 GHz ingress data up to now assuming that the atmosphere consists 85% of H_2 and 15% He[19],[1]. The assumption of a spherically-distributed atmosphere used to compute this $T-p$ profile is known to cause a large error in T, especially in the deep atmosphere, if the oblateness of the planet is large like Jupiter[20], and/or if the isobaric surface shape of the atmosphere is distorted by the zonal winds[21]. If we compare this result with the $T-p$ profile presented in Ref. (19), where both the oblateness of the atmosphere and the zonal winds are accounted for in its analysis, however, the temperature below 100 mbar agrees within 1 K. The difference becomes larger as the pressure becomes smaller, implying that the error is caused not by the oblateness but by the boundary condition used to compute T.

The point of our example is not superiority. It shows good agreement with Lindal et al. (1990) given different model assumptions using a completely independent processing method and independent data set. In that sense it is a new observation and result.

4.2 Multipath Phenomenon through Neptune's Atmosphere

Figure 5 shows the time history of signal power spectra from the Canberra data at 8.4 GHz. The signal level suddenly drops at 8 : 10 : 14, then reappears in about two seconds, with much more complex structure in the spectrum than before. From about 8 : 10 : 23, we can clearly see two split peaks, increasing in frequency difference with time. These spectral features imply a multipath phenomenon in Neptune's atmosphere. The geometry of the spacecraft and the receiving station, and the raypath connecting them, which is bent by the atmosphere of Neptune, define a doppler frequency. For certain vertical refractive index profiles, multiple raypaths with different bending angles connect the transmitter and the receiver at the same time. When this occurs, there are many carriers with different frequencies in a power spectrum of the received signal, each frequency corresponding to a different raypath. Such a signature, though with different time and frequency scales and SNR, has been found in the radio data taken during the Voyager-Uranus encounter. There the raypaths penetrated a methane layer in the Uranian atmosphere where the refractivity scale height was locally smaller than the region above and below it[2]. Therefore the multipath at Neptune also might be created by a cloud layer distribution with a smaller refractivity scale height than the region around it[2]. The importance of the multipath phenomena is that: a) it affect $T-p$ profile, b) it has physical dynamics significance, and c) it is intrinsically interesting for radio propagation studies.

The SNR in the 2.3 GHz signal was too low to detect any multipath. No multipath was observed at either frequency in egress data. Detailed analysis of this phenomenon is under way.

5. Discussion

We stabilized the Canberra 8.4 GHz signal fre-

quency so that we may compute the signal frequency (or phase) and amplitude accurately. Through the processes described in Sects. 3. 2 and 3. 3, the amount of the signal frequency drift was reduced from ~180 Hz down to ~5 Hz (Figs. 1(d), 3(a), (b)), making it possible to reduce the data bandwidth and, consequently, the data volume by more than 30 times. At the same time, the maximum frequency change rate was reduced from ~5 down to 5×10^{-3} Hz/sec above the atmosphere, from ~5 to~0.5 Hz/sec in the atmosphere, and from ~50 to ~3 Hz/sec at the beginning and end of the atmosphere occultation. As a result, we could get about three orders of magnitude better accuracy in the frequency estimation above the atmosphere, and about an order of magnitude better in the atmosphere.

As we can see in Fig. 3(b), the remaining frequency drift still contains short time scale and random variations, which are difficult to remove. Those variation, both in frequency and amplitude, themselves can be a measure of the small scale structure in the atmosphere of Neptune[22].

If the signal frequencies of two different stations are almost the same, it becomes possible to compute the differential signal phase. After compensating the differential phase†, we can array two signals coherently. Coherent arraying of two independently recorded signals such as Canberra and Usuda, can increase the SNR by as much as 1.5 dB without losing time resolution. Consequently, we may extend the $T-p$ profile (Fig. 4) to a higher pressure level, where signal power decreases due to defocussing††. Also we may see the small scale structure in the Neptune's atmosphere with better time resolution without losing SNR.

Acknowledgements

We thank Prof. G. L. Tyler, R. A. Simpson, D. P. Hinson, H. Rand and other staff in the Stanford Center for Radar Astronomy for technical discussion on this work, and Prof. Hayashi and other collaborators in Institute of Space an Astronautical Science for encouragement to pursue the experiment.

References

(1) Lindal G. F., Lyons J. R., Sweetnam D. N., Eshleman V. R., Hinson D. P. and Tyler G. L.: "The Atmosphere of Neptune: Results of Radio Occultation Measurements with the Voyager 2 Spacecraft", Geophys. Res. Lett., **17**, pp. 1733-1736 (1990).

(2) Lindal G. L., Lyons J. R., Sweetnam D. N., Eshleman V. R., Hinson D. P. and Tyler G. L.: "The Atmosphere of Uranus: Results of Radio Occultation Measurements with Voyager 2", J. Geophys. Res., **92**, A13, pp. 14987-15001(1987).

(3) Mizuno E.: "Coherent Signal Arraying of Voyager-Neptune Radio Occultation Data: Data Analysis and Improvement of Physical Measurements", Doctoral dissertation, The University of Tokyo (1991).

(4) Tyler G. L.: "Radio Propagation Experiments in the Outer Solar System with Voyager", Proc. IEEE, **75**, 10, pp. 1404-1431 (1987).

(5) Kliore A. J. and Patel I. R.: "Thermal Structure of the Atmosphere of Venus from Pioneer Venus Radio Occultations", ICARUS, **52**, pp. 320-334 (1982).

(6) Fjeldbo G. and Eshleman V. R.: "Atmosphere of Venus as studied with the Mariner 5 dual radio-frequency occultation experiment", Radio Science, **4**, pp. 879-897 (1969).

(7) Kliore A. J., Cain D. L., Fjeldbo G., Seidel B. L., Sykes M. J. and Rasool S. I.: "The Atmosphere of Mars from Mariner 9 Radio Occultation Measurements", ICARUS, **17**, pp. 484-516 (1972).

(8) Takano, T., Yamamoto Z., Mizuno E., Yamada M., Oh-hashi S., Tsuchiya M., Kawashima N., Hirosawa H. and Hayashi T.,: "Receiving System for Radio Science Experiment of Voyager-2 Spacecraft Neptune Occultation", Trans. IEICE, **J75-B-II**, pp. 47-55 (1992).

(9) Tyler G. L., Marouf E. A., Simpson R. A., Zebker H. A. and Eshleman V. R.: "The Microwave Opacity of Saturn's Rings at Wavelengths of 3.6 and 13 cm from Voyager 1 Radio Occultation", ICARUS, **54**, pp. 160-188 (1983).

(10) Gresh D. L., Marouf E. A., Tyler G. L., Rosen P. A. and Simpson R. A.: "Voyager radio occultation by Uranus' rings. I: Observational results", ICARUS, **78**, pp. 131-168 (1989).

(11) Borutzki S.: "Navigation OD Update and Uncertainties", Jet Propulsion Laboratory Interface Memorandom, Voyager-RSST-90-001 (1990).

(12) Simpson R. A., Private communication (1989).

(13) Thompson A. R., Moran J. M. and Swenson G. W., Jr.,: Interferometry and Synthesis in Radio Astronomy, Wiley-Interscience (1986).

(14) Woo R.: "Radial Dependence Of Solar Wind Properties Deduced From Helios 1/2 And Pioneer 10/11 Radio Scattering Observations", Astrophysical J., **219**, pp. 727-739 (1990).

(15) Asmar S. W.: "Voyager Radio Science Ground Data System Report", presented in the Voyager Radio Science team meeting (Asilomar, USA) held in September (1988).

(16) Asmar S. W. and Eshe P. M.: "Evaluation of the USO Performance—Final Report", Jet Propulsion Laboratory Interface Memorandom, Voyager-RSST-90-121 (1990).

(17) Fjeldbo G., Kliore A. J. and Eshleman V. R.: "The Neutral Atmosphere of Venus as Studied with the Mariner V Radio Occultation Experiments", Astronomical J., **76**, 2, pp. 123-140 (1971).

(18) Eshleman V. R.: "The Radio Occultation Method for the Study of Planetary Atmospheres", Planet. Space Sci., **21**, pp. 1521-1531 (1973).

(19) Tyler G. L., Sweetnam D. N., Anderson J. D., Borutzki S. E., Campbell J. K., Eshleman V. R., Gresh D. L., Gurrola E. M., Hinson D. P., Kawashima N., Kursinski E. R., Levi G. S., Lindal G. F., Lyons J. R., Marouf E. A., Rosen P. A., Simpson R. A. and Wood G. E.: "Voyager Radio Science Observations of Neptune and Triton", Science, **246**, pp. 1466-1473 (1989).

† i.e. make two signals inphase.

†† In the case of 8.4 GHz signals, we cannot expect to extend the profile, because the signal level drops more rapidly than the 2.3 GHz signal in the deep atmosphere (~several bars) due to absorption by ammonia[19].

(20) Eshleman V. R.: "Jupiter's Atmosphere: Problems and Potential of Radio Occultations", Science, **189**, pp. 876-878 (1975).
(21) Lindal G. F., Sweetnam D. N. and Eshleman V. R.: "The Atmosphere of Saturn: An Analysis of the Voyager Radio Occultation Measurements", Astronomical J., **90**, pp. 1136-1146 (1985).
(22) Hinson D. P.: "Strong scintillations during atmospheric occultations: Theoretical intensity spectra", Radio Science, **21**, pp. 257-270 (1986).
(23) Lipa B. and Tyler G. L.: "Statistical and Computational Uncertainties in Atmospheric Profiles from Radio Occultation: Mariner 10 at Venus", ICARUS, **39**, pp. 192-208 (1979).

Appendix: Frequency Estimation Method

Assume the sampled signal has the form

$$x_n = Ae^{2\pi i f_c n \Delta t} \qquad (A \cdot 1)$$

where n is an integer and Δt is the sampling interval. Using a DFT to compute its power spectrum by definition applies a rectangular function to it from time $n\Delta t$ to $n\Delta t + T$ so that the power spectrum in this interval becomes

$$p(f) = A^2 \frac{\sin^2[\pi(f - f_c)T]}{\sin^2[\pi(f - f_c)\Delta t]}. \qquad (A \cdot 2)$$

By fittng this curve to the measured power spectrum of the signal, which includes noise as well as carrier, the optimum f_c and A can be computed[23]. However, as was mentioned in Sect. 3. 1, this method assumes a constant signal frequency over the time period T, which is not necessarily true.

Ei-ichi Mizuno received B. L. A., M. S. and Ph. D. degrees in Physics from the University of Tokyo in 1985, 1987 and 1991, respectively. Since 1986, Dr. Mizuno has been engaged in the radio science experiments of solar corona using the Japanese spacecraft "Suisei", and of Neptune using "Voyager 2". From 1990 to 1991, Dr. Mizuno was a research associate in the Department of Electrical and Computer Engineering, Kanazawa University. Currently, Dr. Mizuno is a research associate at the Institute of Space and Astronautical Science, where he is continuing his work in radio science with Voyager data, and also engaged in the experiment to receive gravitational wave using a laser interferometer.

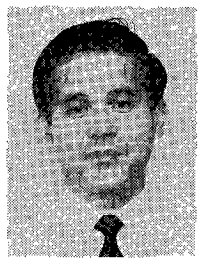

Nobuki Kawashima was born in 1937. Received B. A. Sc. degree in Physics Dep. of Univ. of Tokyo and Ph. D. degree of Univ. of Tokyo in Physics in 1964. He worked as a Research scientist in Japan Atomic Energy Institute from 1964 till 1969 and an Associate Prof. of Institute of Space and Aeronautical Science of Univ. of Tokyo from 1969. The Institute was separated from Univ. of Tokyo in 1981 and he has been Prof. of The Institute of Space and Astronautical Science since 1985. During 1967-68, he was invited from NASA Goddard Space Flight Center as a Research Associate and Vsiting Scientist from European Space Research Institute. He was a Visiting Prof. of Stanford Univ. in 1982. His major activities are Japanese 6-th Scientific Satellite EXOS-B, Space Shuttle SEPAC Project, Voyager-Neptume radio science experiment and various laboratory simulation experiment. Now, he is developing a Laser Interferometer Gravitational Wave Antenna and planning future planetary missions.

Tadashi Takano was born in Tsukuba, Japan in 1945. He received the B.S., M.S. and Ph.D. degrees in electronics engineering from the University of Tokyo, in 1967, 1969 and 1972, respectively. He joined the Electrical Communication Laboratories of Nippon Telegraph and Telephone Public Corporation, in 1972, where he worked with research and development on the antennas for terrestrial relay systems and the Japanese domestic satellite communications system. He moved to the Institute of Space and Astronautical Science, Japan in 1984, where he is now an professor in Radio Tracking. His research interests include antenna engineering, radio wave applications and telecommunication engineering. He received the Yonezawa Award for the study on cross polarization characteristics of aperture antennas, from the Institute of Electronics and Communication Engineers of Japan in 1975. Dr Takano is a member of the Japan Society of Information and Communication Research, and IEEE.

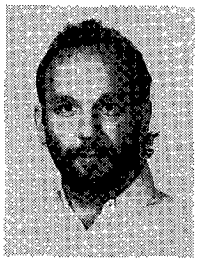

Paul Rosen received B.S. and M.S. degrees in Electrical Engineering from the University of Pennsylvania in 1981 and 1982, respectively. While a doctoral student at Stanford University, Dr. Rosen studied electromagnetic diffraction from Saturn's rings and the interaction of radio waves with gravitationally-induced ring waves. He received a Ph. D. in Electrical Engineering from Stanford in 1989. As a graduate student and post-doctoral scholar at Stanford, Dr. Rosen participated in two planetary encounters, when Voyager flew by Uranus in 1986 and Neptune in 1989. Since March 1990, Dr. Rosen has been with the Electrical Engineering faculty of Kanazawa University continuing his work with Voyager data, and studying very low frequency electromagnetic waves propagating in Earth's magnetosphere observed by Japan's Akebono satellite.